The Version of Record of this manuscript has been published and is available in INORGANIC CHEMISTRY 05 August 2024 https://pubs.acs.org/doi/10.1021/acs.inorgchem.4c01793

6-(6-Methyl-1,2,4,5-tetrazine-3-yl)-2,2‘-bipyridine: A N-donor ligand for the separation of lanthanides(III) and actinides(III)

Gerlinde Greif‡[1], Fynn S. Sauerwein‡[2], Patrik Weßling‡[4], Tamara Duckworth[5], Michael Patzschke[5], Robert Gericke[5], Thomas Sittel[3], Juliane März[5], Andreas Wilden[2], Giuseppe Modolo[2], Petra J. Panak[3,4] and Peter W. Roesky[1,6]*

[1] Institute of Inorganic Chemistry, Karlsruhe Institute of Technology, Engesserstr. 15, 76131 Karlsruhe, Germany; E-mail: roesky@kit.edu

[2] Institute of Fusion Energy and Nuclear Waste Management – Nuclear Waste Management (IFN-2), Forschungszentrum Jülich GmbH, 52428 Jülich, Germany

[3] Institute for Nuclear Waste Disposal, Karlsruhe Institute of Technology (KIT), Hermann-von-Helmholtz-Platz 1, 76344 Eggenstein-Leopoldshafen, Germany

[4] Institute of Physical Chemistry, Heidelberg University, 69120 Heidelberg, Germany

[5] Institute of Resource Ecology, Helmholtz-Zentrum Dresden-Rossendorf, Bautzner Landstraße 400, 01328 Dresden, Germany

[6] Institute of Nanotechnology, Karlsruhe Institute of Technology (KIT), Hermann-von-Helmholtz-Platz 1, 76344 Eggenstein-Leopoldshafen, Germany

E-mail: roesky@kit.edu; ‡ Authors contributed equally.

ABSTRACT

Here we report the synthesis of the 6-(6-methyl-1,2,4,5-tetrazine-3-yl)-2,2‘-bipyridine (MTB) ligand, that has been developed for lanthanide/actinide separation. A multi-method study of the complexation of MTB with trivalent actinide and lanthanide ions is presented. Single crystal X-ray diffraction measurements reveal the formation of $[Ce(MTB)_2(NO_3)_3]$, $[Pr(MTB)(NO_3)_3H_2O]$, and $[Ln(MTB)(NO_3)_3MeCN]$ (Ln = Nd, Sm, Eu, Gd). In addition, the complexation of Cm(III) with MTB in solution was studied by time-resolved laser fluorescence spectroscopy. The results show the formation of $[Cm(MTB)_{1\text{-}3}]^{3+}$ complexes, which occurs in two different isomers. Quantum chemical calculations reveal an energy difference between these isomers of 12 kJ mol^{-1}, clarifying the initial observations made by TRLFS. Furthermore, QTAIM analysis of the Cm(III) and Ln(III) complexes was performed, indicating a stronger covalent contribution in the Cm-N interaction compared to the respective Ln-N interaction. These findings align well with extraction data showing a preferred extraction of Am and Cm over lanthanides (e.g., max. $SF_{Am/Eu} = 8.3$) at nitric acid concentrations < 0.1 mol L^{-1} HNO_3.

INTRODUCTION

Efficiently handling the separation and treatment of lanthanides (Ln) and actinides (An) in radioactive waste remains a significant challenge in nuclear waste management. Due to the striking similarities among these elements, this process has become significantly complex.[1] Radioactive waste is produced in various domains, most notably during electricity generation in nuclear power plants, both during operational phases and decommissioning. A critical aspect of the nuclear fuel cycle is addressing the long-term radiotoxicity and heat generation from spent nuclear fuel. These factors are preliminary caused by plutonium and the minor actinides (Np, Am, and Cm) and become a major concern after approximately 100 years of storage.[2] Various countries adopt differing strategies for disposal including direct disposal of fuel or

exclusive disposal of vitrified, highly active residual waste after reprocessing through the PUREX (Plutonium Uranium Reduction Extraction) process. This methodology segregates uranium and plutonium for re-use as mixed oxide (MOX) nuclear fuel.[3] However, several nations strive not only to separate and recycle uranium and plutonium but also to include the minor actinides neptunium, americium, and curium.[4-8] The fundamental concept involves segregating plutonium and minor actinides, with their long-lived, toxic isotopes, from high-level radioactive waste through partitioning. Subsequently, these elements undergo neutron fission, transmuting into short-lived or stable isotopes. Given that certain lanthanides possess substantial neutron absorption cross-sections, their separation from trivalent actinides is crucial for effective transmutation. In this pursuit, solvent extraction stands out as a promising approach, requiring the use of well-designed complexing agents. While conventional oxygen-donor ligands may lack the desired selectivity, nitrogen or sulfur-donor ligands, with their softer characteristics, display a significantly higher selectivity for trivalent minor actinides compared to the lanthanides.[4,9-11] Current developments of mixed N,O-donor ligands aim at combining the high metal binding affinity of O-donor ligands with the desired selectivity of N-donor ligands.[12-17] Unfortunately, most of these compounds are ineffective when extracting from solutions with a high nitric acid concentration (> 0.5 mol L^{-1} HNO_3), which is necessary for the PUREX process. Alkyl-substituted 2,6-ditriazinylpyridines (BTP),[18-20] alkylated 6,6'-ditriazinylbipyridines (BTBP),[21-23] and their phenanthroline derivatives (BTPhen)[24,25] have been developed and can directly extract trivalent actinides from nitric acid solutions with a high selectivity over the lanthanides. Besides the reprocessing of spent nuclear fuel, the development of new ligands for the An/Ln separation is also of interest for radiopharmaceutical applications, e.g., for the purification of ^{225}Ac from Ln radionuclides.[26,27]

Despite extensive insights into the complexation and extraction attributes of numerous BT(B)P-type ligands, the molecular selectivity of certain ligands is not yet fully understood. Previous advances in extraction performance have largely resulted from empirical “trial and

error" approaches. To gain a deeper understanding of the relationship between bond properties, structures and extraction performance, a novel asymmetric ligand based on 6-(tetrazol-5-yl)-2,2′-bipyridine (HN_4bipy)[28] was synthesized and studied. This work describes the synthesis of 6-(6-methyl-1,2,4,5-tetrazine-3-yl)-2,2‘-bipyridine (MTB) and its coordination chemistry with cerium, praseodymium, neodymium, samarium, europium, and gadolinium nitrates. Integral thermodynamic data pertaining to the complex formation of MTB with lanthanides (Ln(III)) and curium(III) was methodically obtained through time-resolved laser fluorescence spectroscopy (TRLFS), solvent extraction and computational studies.

RESULTS AND DISCUSSION

SYNTHESIS OF MTB AND ITS LANTHANIDE COMPLEXES

The MTB ligand was synthesized through a four-step protocol, using 2,2‘-bipyridine as initial starting material (Scheme 1). In the first step, 2,2‘-bipyridine was oxidized to 2,2‘-bipyridine-N-oxide in nearly quantitative yield.[29,30] Subsequently, for the synthesis of 2,2‘-bipyridine-6-carbonitrile, an N-oxide cyanation of 2,2‘-bipyridine-N-oxide was performed using trimethylsilyl cyanide and benzoyl chloride, employing a modified Reissert-Henze reaction.[30,31]

The synthesis of the tetrazine moiety in the third step followed a procedure described by Polezhaev *et al.*[32] The conversion of 2,2‘-bipyridyl-6-carbonitrile into the intermediate 6-(6-methyl-1,2-dihydro-1,2,4,5-tetrazine-3-yl)-2,2‘-bipyridine was accomplished by a reaction employing hydrazine hydrate, sulfur, and acetonitrile in ethanol. The final step of the synthesis involved the reaction of (6-methyl-1,2-dihydro-1,2,4,5-tetrazine-3-yl)-2,2‘-bipyridine with sodium nitrite in a mixture of acetic acid and water. After purification, the desired ligand showed a characteristic purple color. By optimizing the reaction conditions, the ligand was obtained with a total yield of 51% over all four synthetic steps. The successful synthesis of

MTB was confirmed by ^{1}H and $^{13}C\{^{1}H\}$ NMR spectroscopy, ESI mass spectrometry and elemental analysis (SI, Figures S3-S4).

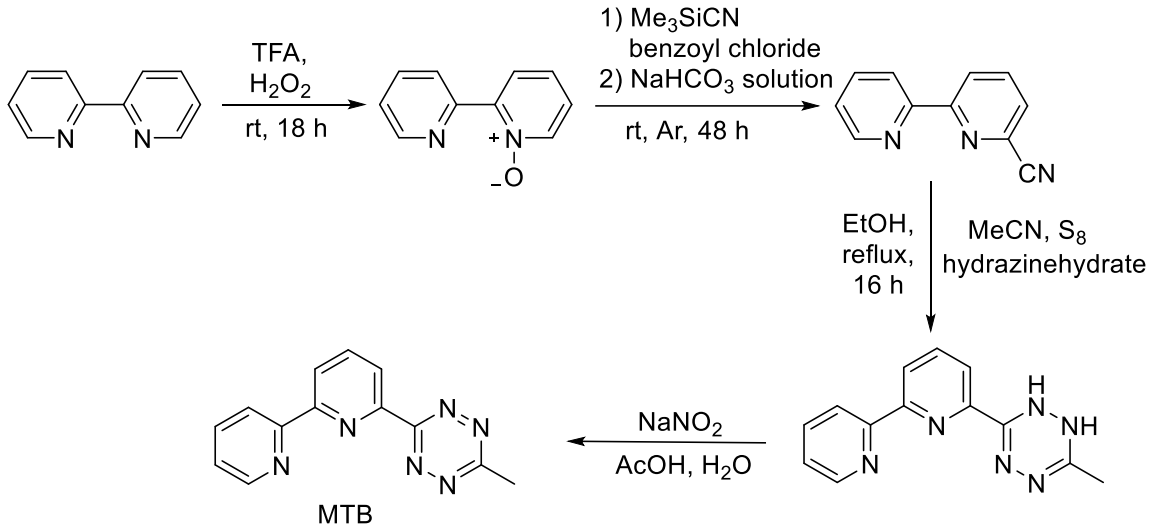

Scheme 1: Synthesis of 6-(6-methyl-1,2,4,5-tetrazine-3-yl)-2,2‘-bipyridine (MTB).

In addition, the molecular structure of MTB in the solid-state was confirmed by single crystal X-ray diffraction (SCXRD). MTB crystallizes in the monoclinic space group $P2_1/c$ with four molecules in the unit cell (Figure 1). The N-N distances in the tetrazine ring are 1.331(2) Å (N3-N4) and 1.317(3) Å (N5-N6), and the N-C distances are 1.336(3) Å (N3-C11), 1.338(3) Å (N4-C12), 1.336(3) Å (N5-C12), and 1.348(2) Å (N6-C11). Therefore, the N-C distances in the bipyridine are very similar to the two related ligand systems, HN_4bipy and 4,4′-di-*tert*-butyl-6-(1*H*-tetrazol-5-yl)-2,2′-bipyridine (HN_4′bubipy).[28,31] This emphasizes the structural similarity between MTB and these referenced ligand systems.

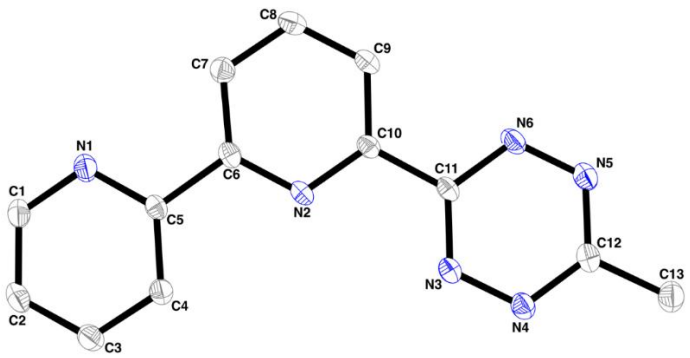

Figure 1: Molecular structures of MTB in the solid-state. Ellipsoids are drawn to encompass 50% probability. Hydrogen atoms are omitted for clarity. Selected bond lengths and angles can be found in the supporting information (Figure S12).

Since the MTB ligand was designed for extraction studies, we aimed for a dynamic coordination in solution. However, this led to a pronounced dissociation of the complexes in solution. To isolate the desired lanthanide complexes, a synthesis protocol was therefore needed that aims to reduce the dissociation of the complexes in solution. For this purpose, the $[Ln(NO_3)_3 \cdot 6H_2O]$ (Ln = Ce, Pr, Nd, Sm, Eu, Gd) precursors were first suspended in THF. This allowed the THF to be first coordinated to the lanthanide. The solvent was then removed under reduced pressure. MTB was then added to the mixture and dissolved in acetonitrile. The solutions were allowed to stand at room temperature. After several days, crystals of the corresponding complexes, $[Ce(MTB)_2(NO_3)_3]$ (**1**), $[Pr(MTB)(NO_3)_3H_2O]$ (**2**), and $[Ln(MTB)(NO_3)_3MeCN]$ (Ln = Nd (**3**), Sm (**4**), Eu (**5**), Gd (**6**)) suitable for SCXRD analysis were obtained (Schemes 2-3). All compounds crystallize in the triclinic space group $P\bar{1}$.

The cerium complex **1** (Scheme 2) exhibits a unique 1:2 coordination (Cer:MTB). This contrasts with the other compounds **2-6** (Scheme 3), where only one MTB molecule coordinates. The Ce atom in **1** has a coordination number of twelve due to the bonding with six nitrogen atoms of two MTB molecules and six oxygen atoms of three coordinating nitrate ions. In addition, there are 2.5 non-coordinating acetonitrile molecules present in the unit cell, with one MeCN being located on a center of inversion along the crystallographic a-axis.

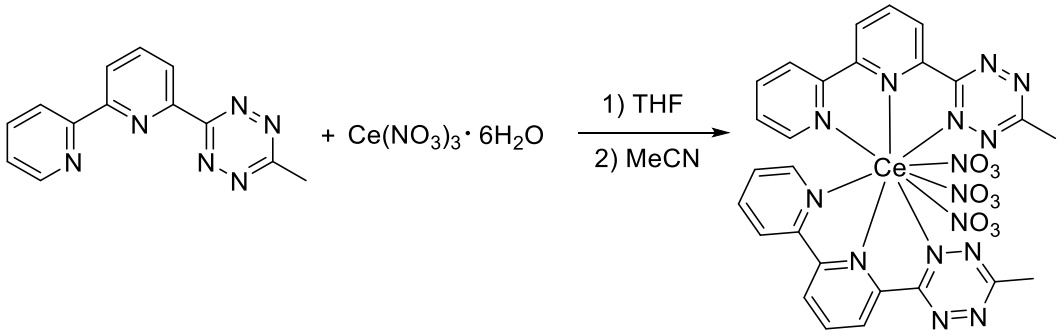

Scheme 2: Synthesis of the cerium complex $[Ce(MTB)_2(NO_3)_3]$ (**1**).

In contrast to **1**, the lanthanide ion in compounds **2-6** is coordinated by only one MTB molecule. In these compounds, the ten-fold coordinated metal atom is bound by three nitrogen atoms from the ligand, six oxygen atoms from three bidentate nitrate ions, and one monodentate coordinating solvent molecule (water in **2**, acetonitrile in **3-6**) (Scheme 3).

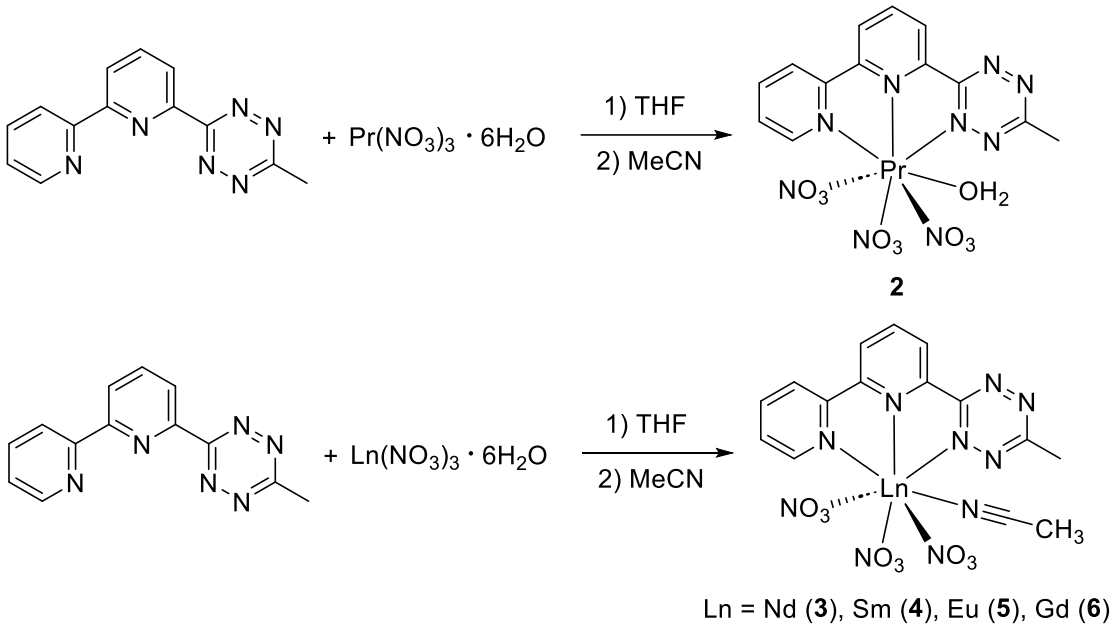

Scheme 3: Synthesis of the complexes **2-6**.

Figures 2 and 3 show the solid-state molecular structures of the complexes **1**, **2**, and **6**. Molecular structures of all compounds **1-6**, including the associated data, can be found in the supporting information (Figures S13-S18). The bond distances from the coordinating nitrogen atoms to the different lanthanide atoms were examined (Table 1). In compound **1** (Figure 2), these distances range from 2.6 to 2.7 Å, which is similar to the bond distances in the reported

compound $[Sm(N_4bipy)_2(OH)(H_2O)_2]$.[28] It is interesting to note that in $[Sm(N_4bipy)_2(OH)(H_2O)_2]$[28] the smallest bond distance is attributed to the nitrogen in the tetrazole moiety, whereas in compound **1** the largest bond distance originates from the nitrogen atom within the tetrazine ring (Ln1-N3/N9), which is a result of the strain caused by the different ligand geometries. In contrast to **1**, the coordinating Ln-N bond distances in complexes **2**-**6** are significantly shorter (Table 1, Figures 2 and 3, Figures S14-S18). This phenomenon is due to the coordination of only one MTB molecule, which leaves more space, allowing a closer coordination of the ligand. The bond distances are similar to those of the reported complex $[Sm(N_4{}^t bubipy)(NO_3)_3(H_2O)]^-[HN_4{}^t bubipyH]^+$, where the central atom is also coordinated by only one ligand molecule.[31] Again the largest distances are observed between the tetrazine and the metal atom (Ln1-N3, Table 1).

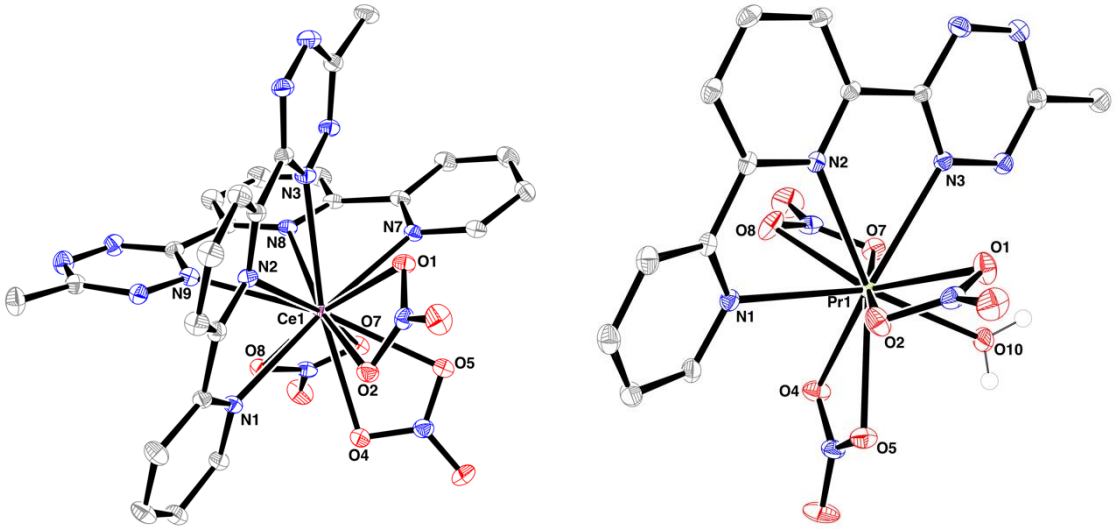

Figure 2: Molecular structures of $[Ce(MTB)_2(NO_3)_3]\cdot 2.5NCMe$ (**1**) and $[Pr(MTB)(NO_3)_3(H_2O)]\cdot NCMe$ (**2**) in the solid-state. Ellipsoids are shown at 50% probability level. Carbon bound hydrogen atoms and non-coordinating solvent molecules are omitted for clarity. Selected bond lengths and angles can be found in the supporting information (Figures S13-S14).

The Ln-N bond distances in complexes **2**-**6**, as shown in Table 1, display the expected decrease of distance between the ligand and the central atom with decreasing lanthanide ionic

radii. Only in the case of complex **2**, the bond distance Ln1-N3 is shorter than in complex **3**. This can be attributed to the coordination of a water molecule instead of acetonitrile, as decrease in bond length with respect to the ionic radii is also observed for the coordinated nitrogen atom of acetonitrile in compounds **3**-**6** (Figure 3, Figures S15-S18).

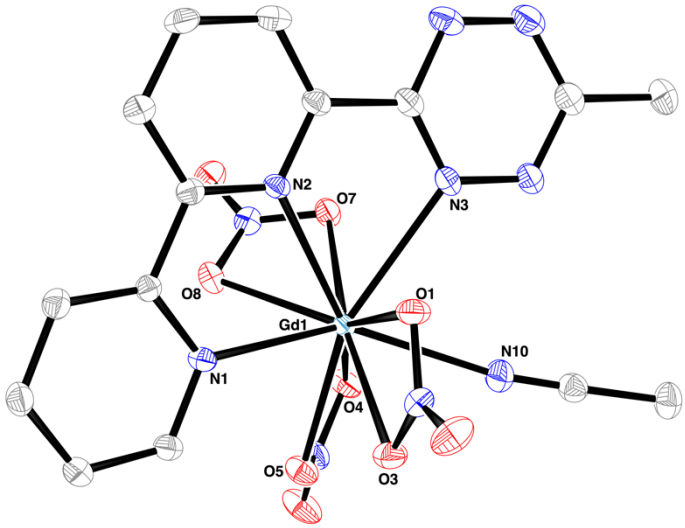

Figure 3: Molecular structures of [Gd(MTB)$(NO_3)_3$(NCMe)] (**6**) in the solid state. Ellipsoids are drawn to encompass 50% probability. Hydrogen atoms are omitted for clarity. Selected bond lengths and angles can be found in the supporting information (Figure S18).

Table 1: Comparison of selected bond distances (in Å) of the coordinated nitrogen atoms to the lanthanide atom bite angle (in deg).

Compound	**Ionic radius, c,n, 9[33]**	**Ln1-N1/N7**	**Ln1-N2/N8**	**Ln1-N3/N9**	**N1-Ln-N3**
1	Ce^{3+} = 1.196	2.701(2) 2.688(2)	2.769(2) 2.756(2)	2.788(2) 2.770(2)	115.7(15) 116.59(5)
2	Pr^{3+} = 0.99	2.623(2)	2.630(2)	2.626(2)	124.15(6)
3	Nd^{3+} = 0.98	2.558(2)	2.602(2)	2.686(2)	123.80(6)
4	Sm^{3+} = 0.96	2.535(2)	2.569(2)	2.669(2)	124.87(7)
5	Eu^{3+} = 0.94	2.521(2)	2.557(2)	2.661(2)	125.38(6)

6	Gd^{3+} = 0.94	2.504(2)	2.528(2)	2.649(2)	126.07(6)

The bond distances of the coordinating nitrate oxygen atoms to the central atom of the individual compounds are all in the range from 2.44(2) to 2.58(2) Å. They are also similar to the corresponding bond distances in the reported complex $[Sm(N_4{}^t bubipy)(NO_3)_3(H_2O)]^-[HN_4{}^t bubipyH]^+$.[31] As expected, complex **1** exhibits slightly larger Ln-O distances, ranging from 2.62(14) to 2.69(14) Å due to the higher coordination number. This contrast in bond lengths, particularly evident in complex **1**, illustrates the difference between the coordination of one or two ligands to the lanthanide ion. When comparing the bite angles between the outer coordinating nitrogen atoms of the ligand and the respective central atom, an increase in the angle is observed with decreasing ionic radius of the central lanthanide, as shown in Table 1. This trend is also expected for compounds **3**-**6**. However, complex **2** deviates from this trend due to structural differences and shows a larger N1-Ln-N3 bite angle. As expected, complex **1**, with bite angles of 115.7(15)° and 116.6(1)°, is significantly smaller due to the double coordination of the ligand. In addition to single crystal X-ray structural analysis, IR spectra (SI, Figures S5-S11) and ESI mass spectra of MTB and compounds **1**-**6** were measured. However, only the nitrates and the dissociated ligand were visible in the ESI-MS spectra.

TRLFS STUDIES

The complexation of Cm(III) with MTB in solution was studied in 2-propanol containing 50 vol.% H_2O using time-resolved laser fluorescence spectroscopy (TRLFS). First, complexation kinetics were studied by setting the MTB concentration to 3.42×10^{-3} mol L^{-1} and recording Cm(III) emission spectra as a function of time after addition of the ligand. The emission spectra resulting from the transition $^6D'_{7/2} \rightarrow {}^8S'_{7/2}$ are shown in Figure 4.

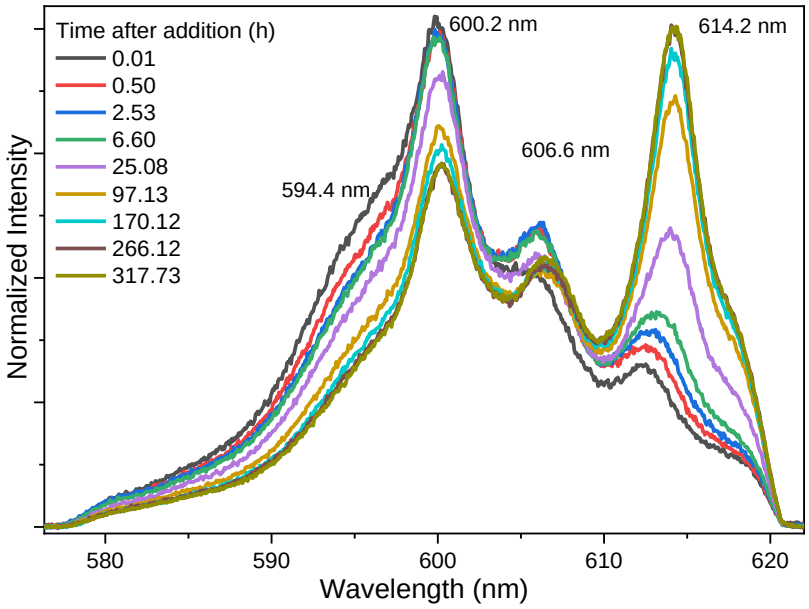

Figure 4: Normalized Cm(III) emission spectra in 2-propanol containing 50 vol.% H_2O as a function of time after addition of MTB. $[Cm(III)]_{ini} = 10^{-7}$ mol L^{-1}; [MTB] = 3.42×10^{-3} mol L^{-1}.

Immediately after the addition of MTB three emission bands at 600.2 nm, 606.6 nm and 614.2 nm were observed next to the one of the solvated Cm(III) ion (594.4 nm).[34] With time, the intensity of the emission bands at 594.4 nm and 600.2 nm decreased, while the intensity of the band at 614.2 nm increased. Chemical equilibrium was reached 266 h after addition of MTB, as indicated by constant emission spectra after this point in time. The complexation kinetics are comparable to the previously examined structurally similar ligands 6-(5,6-dipentyl-1,2,4-triazin-3-yl)-2,2'-bipyridine (C5-hemi-BTP)[35] and 2,6-bis(6-propyl-1,2,4,5-tetrazin-3-yl)pyridine (*n*Pr-tetrazine)[36] (Scheme 4).

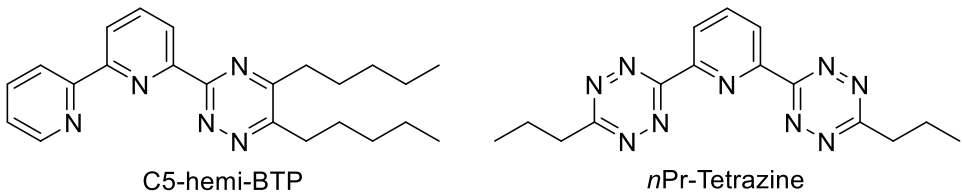

Scheme 4: Molecular structures of C5-hemi-BTP and *n*Pr-tetrazine.

Moreover, by comparison with the emission bands of the $[Cm(C5\text{-hemi-BTP})_n]^{3+}$ (n = 1: λ_{max} = 599.9 nm; n = 2: λ_{max} = 607.3 nm; n = 3: λ_{max} = 612.8 nm) and $[Cm(n\text{Pr-tetrazine})_n]^{3+}$

complexes (n = 1: λ_{max} = 599.7 nm; n = 2: λ_{max} = 606.0 nm; n = 3: λ_{max} = 611.0 nm) one can conclude that the observed emission bands belong to the $[Cm(MTB)_n]^{3+}$ complexes (n = 1-3). To determine the sequential formation of the different Cm(III) species with MTB, emission spectra were recorded as a function of the MTB concentration after the chemical equilibrium was reached. Based on our kinetic study emission spectra were recorded after an equilibration time of 12 days. Figure 5 shows the normalized Cm(III) emission spectra in 2-propanol containing 50 vol.% H_2O as a function of the MTB concentration.

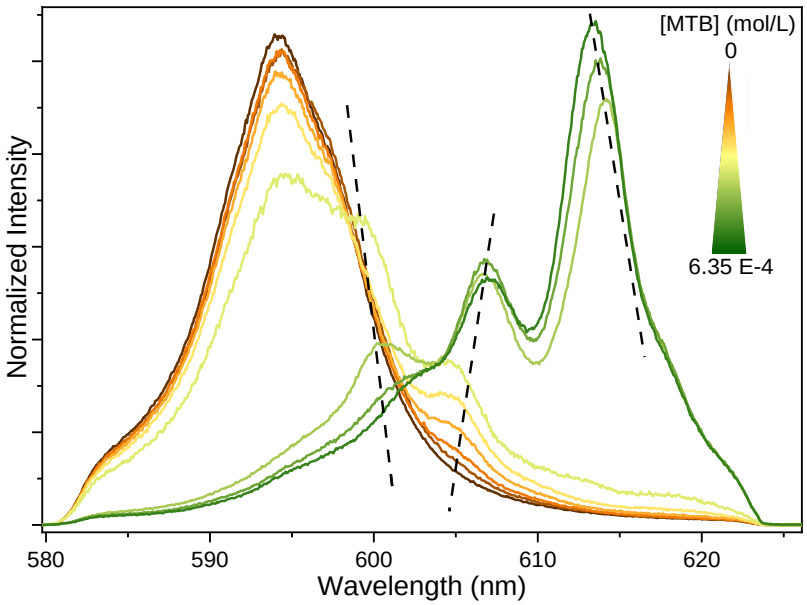

Figure 5: Normalized Cm(III) emission spectra in 2-propanol containing 50 vol.% H_2O as a function of the MTB concentration. $[Cm(III)]_{ini} = 10^{-7}$ mol L^{-1}.

In absence of MTB, the solvated Cm(III) spectrum at 594.4 nm is observed. Upon stepwise addition of MTB, the development of the three emission bands of the $[Cm(MTB)_n]^{3+}$ (n = 1-3) complex species can be observed Normally, the emission maximum remains constant for each complex species. However, the observed emission maxima shift slightly with increasing ligand concentration from 599.5 nm to 600.5 nm for the $[Cm(MTB)]^{3+}$ species, from 606.9 nm to 604.9 nm for the $[Cm(MTB)_2)]^{3+}$ species, and from 614.2 nm to 612.7 nm for the $[Cm(MTB)_3]^{3+}$ species, as indicated by the dashed lines in Figure 5. Shifts in the emission bands

of a complex species can sometimes arise due to minor changes in the second coordination sphere, typically amounting to less than 1 nm.[37] However, the shifts observed for the $[Cm(MTB)_n]^{3+}$ (n = 1-3) complexes are in the range of 1 to 2 nm. For lack of constant emission maxima, spectral analysis through peak deconvolution was not feasible. This prevented the determination of complex stability constants. The shifting emission maxima might be explained by the formation of different configuration isomers of $[Cm(MTB)_n]^{3+}$ (n = 2-3) complexes. This is supported by complexation studies of another asymmetric ligand, C5-hemi-BTP (Figure 4, left). The emission bands of the $[Cm(C5\text{-}hemi\text{-}BTP)_n]^{3+}$ (n = 1-3) complexes remain unchanged regardless of the C5-hemi-BTP concentration.[35] Unlike MTB, C5-hemi-BTP has long alkyl chains. These chains may cause steric hindrance, resulting in the formation of only one complex isomer. In contrast, the absence of long chains in the MTB ligand may allow the formation of different stable complex isomers, explaining the observed emission band shift. As highlighted in Figure 6, different complex isomers are possible for the $[Cm(MTB)_3]^{3+}$ complex. These vary in the spatial orientation of the terminal methyl groups.

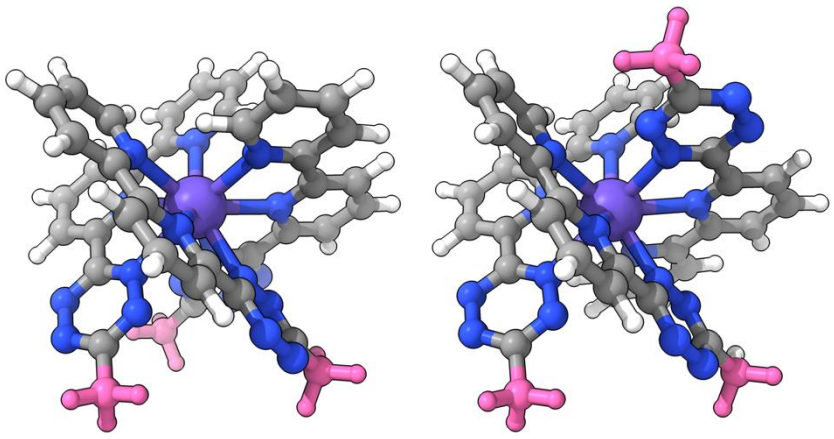

Figure 6: Two configuration isomers of $[Cm(MTB)_3]^{3+}$.

COMPUTATIONAL RESULTS

To gain further insight into the binding mode of the MTB ligand, a series of calculations was performed. Computational details can be found in the supporting information. To

compare the bonding for all lanthanides used in this study, the structure of the hypothetical Ce and Pr complexes with the same composition as **3**-**6** were calculated. The calculated Ln-N distances can be found in Table 2.

Table 2: Calculated Ln-N bond distances (in Å) for the [Ln(MTB)$(NO_3)_3$(MeCN)] complexes. The numbering is consistent with Table 1. Additionally, the bond length to acetonitrile (N10) is added.

Ln	**Ln1-N1**	**Ln1-N2**	**Ln1-N3**	**Ln1-N10**
Ce	2.639	2.719	2.746	2.704
Pr	2.636	2.706	2.717	2.686
Nd	2.607	2.671	2.713	2.643
Sm	2.587	2.653	2.706	2.619
Eu	2.589	2.642	2.687	2.600
Gd	2.553	2.610	2.688	2.583

Comparing the calculation to the experiment, it is apparent, that the Ln-N bond lengths are consistently overestimated by up to 0.07 Å, most likely due to crystal packing effects. The somewhat large size of the deviation can be attributed to a rather soft bonding of the MTB ligand. There is no difference in the trends though and the bond length alteration across the series is consistent with the ionic radii of the involved lanthanide. Especially the hypothetical Ce complex with only one MTB ligand shows the expected bonding pattern and the expected shorter bonds as the synthesized Ce complex with two MTB ligands. The bond length for the attached acetonitrile is always the second shortest, longer only than the bond to the terminal pyridine ring. This is indicative of a relatively strong interaction to the acetonitrile. These bond distance trends already suggest that there is no strong deviation from the expected atomic-orbital occupation numbers. The results of the corresponding NBO analysis are shown in Table 3.

Table 3: NBO analysis data for the [Ln(MTB)$(NO_3)_3$(MeCN)] complexes. Given are the orbital occupation numbers and NBO charges for the lanthanides.

Ln	Orbital occupation	q(Ln)
Ce	[core]6s(0.22)4f(1.14)5d(0.97)	1.58
Pr	[core]6s(0.23)4f(2.11)5d(0.96)	1.61
Nd	[core]6s(0.23)4f(3.11)5d(1.01)	1.55
Sm	[core]6s(0.24)4f(5.19)5d(1.03)	1.42
Eu	[core]6s(0.25)4f(6.25)5d(0.99)	1.41
Gd	[core]6s(0.26)4f(7.03)5d(1.05)	1.55

The charge of the lanthanide varies only slightly across the series and deviates strongly from the formal charge +3. This suggests, of course, some electron transfer from the ligands to the central ion, as can also be seen by the orbital occupation numbers. Slightly larger excess *f*-occupations are found for Sm and Eu than for the other lanthanides, but not enough to expect a different bonding mode. A sign of orbital interaction between the lanthanide and the ligands can be obtained from a QTAIM analysis, especially the delocalization index (DI) is a useful tool in this respect. In Table 4 the DI's for the Ln-N interactions are given.

Table 4: Delocalization indices (DI) for the Ln-N bonds in [Ln(MTB)$(NO_3)_3$(MeCN)] complexes. The numbering is consistent with Table 1.

Ln	DI(Ln1-N1)	DI(Ln1-N2)	DI(Ln1-N3)	DI(Ln1-N10)
Ce	0.228	0.184	0.174	0.172
Pr	0.218	0.179	0.166	0.172
Nd	0.220	0.179	0.158	0.178
Sm	0.216	0.179	0.150	0.174
Eu	0.205	0.174	0.153	0.175
Gd	0.216	0.182	0.143	0.174

The DI values reveal only a small degree of covalency between the lanthanides and the nitrogen atoms of the ligands. Additionally, the electron density at the bond critical point is rather low with values between 0.03 and 0.04. This is indicative of a charge transfer character of the Ln-N bonds. The values should be compared to the data for the $[Cm(MTB)_3]^{3+}$ complex. Here, we find three MTB ligands attached to the central ion, but the DI's are still larger (0.261 for Cm-N1, 0.253 for Cm-N2, and 0.236 for Cm-N3) than the DI's for the lanthanides. Furthermore, the electron density at the bond critical point is consistently above 0.04. On the other hand, for the synthesized cerium complex **1**, DI's of 0.190, 0.127 and 0.106 are found. This shows that the bond between Ce and one MTB molecule is weakened by attaching a second MTB moiety. This is due to sterical crowding and gives a clear indication that a 1:3 complex between Ce and MTB cannot be formed.

It is interesting to note that the DI's for the MeCN-Ln interaction are lower than the values for the Ln-N2 interactions, although the MeCN-Ln bond distances are shorter. This is due to the smaller MeCN being able to penetrate deeper into the coordination sphere, whereas the MTB ligand is not flexible enough to get as close. For all calculated complexes the bond distances are always in the order Ln-N1 < Ln-N2 < Ln-N3. This fact is best explained by looking at the atomic charges of the free ligand as given in Figure 7. The shortest bond forms, as expected, with the nitrogen that possesses the highest electron density.

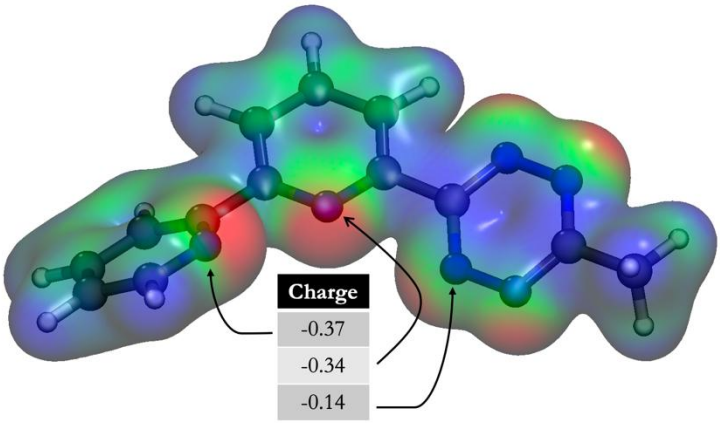

Figure 7: Mapped electrostatic potential and NBO charges for the free MTB ligand.

As noted before, the Cm 1:3 complex shows higher DI's consistent with a more covalent bonding between the actinide and the ligand. With a 1:3 ratio, two different isomers are possible. These are depicted in Figure 6. The calculated ΔG value between the two structures is only 12.2 kJ mol^{-1} in favor of the syn structure. Using a simple Boltzmann distribution this would indicate, that roughly 1% of the dissolved complex is in the anti-form and 99% in the syn-form. With respect to the performed TRLFS studies it is interesting to look at the absorption spectrum of the two $[Cm(MTB)_3]^{3+}$ isomers (vide infra). These spectra were calculated at the CASSCF level with a (7,7) active space, i.e. considering only the *f*-orbitals. The resulting spectrum only shows transitions between those orbitals and does not contain any ligand excitations. Spectra calculated at the CASSCF level give good relative peak positions, but the absolute values are not representative, hence these spectra are sometimes shifted. This has not been done here as the salient point is the difference between the two isomers. The calculated spectra of the two $[Cm(MTB)_3]^{3+}$ isomers are depicted in Figure 8.

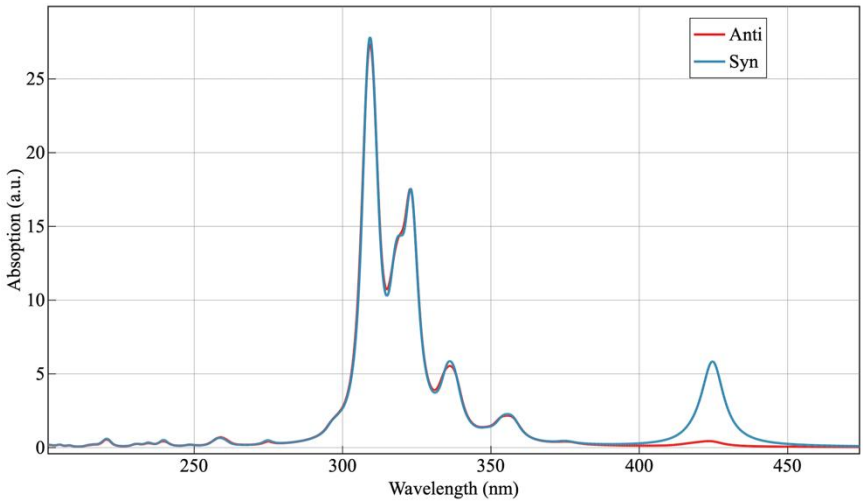

Figure 8: Calculated SO-CAS absorption spectra of the two $[Cm(MTB)_3]^{3+}$ isomers.

The two spectra are almost identical, apart from the peak around 425 nm. This peak corresponds to the transition that is used for excitation in the TRLFS studies (λ_{exp} = 396.6 nm). The intensity of the peak for the anti-form is only ~10% compared to the syn-form. As the syn-

form is the more stable isomer, this should not impact the TRLFS studies in the long-time regime but might influence it when the complex is formed statistically in the beginning of the complexation reaction, as one could expect a higher concentration of the anti-isomer during that time.

SOLVENT EXTRACTION STUDIES

MTB was tested as an extractant for trivalent *f*-block metal ions. Commonly, aliphatic diluents are used in nuclear solvent extraction processes. Therefore, in a preliminary test, the approximate maximum solubility of MTB in different diluents was determined (SI, Table S2). MTB solubility in the aliphatic diluents *n*-dodecane and *n*-octanol is very low (< 3 mmol L^{-1}), but for aromatic diluents, MTB solubility was found to increase with increasing polarity in the order *tert*-butylbenzene < phenyl trifluoromethyl sulfone (FS-13) < toluene < chlorobenzene < nitrobenzene. After shaking the MTB solutions in different organic diluents against different HNO_3 concentrations and centrifugation, an increasingly pink coloration of the aqueous phase was observed (SI, Figures S19-S21). This is attributed to an increased stripping of MTB into the aqueous phase with increasing nitric acid concentration. Although MTB is not soluble in water, it can be dissolved in 0.1 mol L^{-1} HNO_3 solution up to ca. 48 mmol L^{-1} (SI, Table S2). Figure 9 shows Eu, Am, and Cm distribution ratios for the extraction with MTB in *tert*-butylbenzene with and without addition of the lipophilic anion source 2-bromodecanoic acid (HA) in the range from 10^{-4} to 10^{-1} mol L^{-1} HNO_3. Without HA, MTB was unable to extract trivalent metal ions ($D < 10^{-3}$). With addition of 0.5 mol L^{-1} HA to the organic phase, extraction of trivalent metal ions into the organic phase was observed. Maximum distribution ratios ($D_{Am} = 123$, $D_{Cm} = 87$, $D_{Eu} = 18$) were reached at the lowest tested nitric acid concentration (6×10^{-4} mol L^{-1} HNO_3). The distribution ratios decrease with increasing nitric acid concentration. This is typical for a cation-exchange mechanism since the equilibrium shifts to the reactant side with increasing proton concentration (eq. 1). Significant extraction with MTB

with distribution ratios $D > 1$ is only possible at low nitric acid concentrations $< 5\times10^{-2}$ mol L^{-1} HNO_3. Unfortunately, MTB gives low distribution ratios at higher nitric acid concentrations, which are more relevant for nuclear fuel reprocessing. HA itself extracts trivalent *f*-block ions to a significant extent only at nitric acid concentrations $< 10^{-3}$ mol L^{-1} HNO_3[38,39] (SI, Figure S22) but works as a synergist for extraction with N-donor ligands *via* a cation-exchange mechanism[40-42]:

$$M^{3+}{}_{aq} + 3\,HA_{org} + n\,MTB_{org} \rightleftharpoons [MA_3MTB_n]_{org} + 3\,H^{+}{}_{aq} \qquad \text{eq. 1}$$

HA is known to dissociate in the aqueous phase with the 2-bromodecanoate anions forming complexes with the trivalent metal ions that can then be transferred into the organic phase. Nilsson *et al.* investigated some chemical properties of 2-bromodecanoic acid that influence its extraction properties.[43] On the one hand, HA forms dimers and the dimerization is usually more prominent in nonpolar diluents. On the other hand, monomeric HA is distributed between both phases, whereas HA generally interacts stronger with more polar diluents and thus the distribution into the aqueous phase is suppressed. Both competing properties influence the concentration of dissociated HA in the aqueous phase.[43] Figure 10 compares the distribution ratios of Am(III) and Eu(III) for MTB extraction in *tert*-butylbenzene, toluene and nitrobenzene with addition of 0.5 mol L^{-1} HA. Although MTB solubility is higher in more polar solvents (nitrobenzene > toluene > *tert*-butylbenzene, SI Table S2), this does not result in higher distribution ratios. Instead, distribution ratios were found to decrease with increasing solvent polarity (*tert*-butylbenzene > toluene > nitrobenzene). This observation can be explained by a reduced synergistic complexation of the 2-bromodecanoate anion when using more polar solvents which outperforms the better MTB solubility. To further study the influence of HA, Am and Eu distribution ratios for extraction with 0.5 mol L^{-1} HA alone (without MTB) were compared in different diluents (SI, Figure S22) and found to follow the same order *n*-dodecane > *tert*-butylbenzene > toluene > nitrobenzene as observed in Figure 10. Thus, the synergistic effect of HA is expected to be highest in nonpolar diluents, as was also noticed for other ligands,

e.g., 2,6-bis(5-(2,2-dimethylpropyl)-1*H*-pyrazol-3-yl)pyridine (C5-BPP) exhibiting highest distribution ratios for extraction in kerosene with HA.[42] Figures 9 and 10 show the metal ion distribution ratios as a function of the acidity. Slope analysis is performed to determine the number of exchanged protons. Since the exchange of three protons is expected (eq. 1), slopes of -3 are expected. However, slopes of -2.3 to -2.5 are found. This deviation can result from non-ideal experimental conditions, as concentrations instead of activities are used, or yet unknown differences in the mechanism, *e.g.* protonation of the ligand itself. At higher acidities ($> 10^{-2}$ mol L^{-1} HNO_3), steeper slopes were observed, which are probably caused by an increased solubility of MTB in nitric acid solution (SI, Figure S19-S21), as discussed above. The Am(III)/Eu(III) selectivity decreased with increasing solvent polarity in the order *tert*-butylbenzene > toluene > nitrobenzene with max. $SF_{Am/Eu}$ = 8.3 in *tert*-butylbenzene, max. $SF_{Am/Eu}$ = 7.7 in toluene, and max. $SF_{Am/Eu}$ = 5.8 in nitrobenzene. This is comparable to other 1,2,4,5-tetrazinyl extractants such as *n*Pr-tetrazine ($SF_{Am/Eu}$ = 9)[44] but considerably lower compared to bis(1,2,4-triazin-3-yl)pyridines such as *n*Pr-BTP ($SF_{Am/Eu}$ > 100).[20] MTB showed no enhanced selectivity for the separation of Am from Cm ($SF_{Am/Cm}$ = 1.4). Furthermore, the extraction of all lanthanides (w/o Pm, including Y) was tested (SI, Figure S23). Distribution ratios increase from La to Sm and then remained at the same level until Lu. In general, Ln(III) distribution ratios are all within one order of magnitude showing a poor selectivity of MTB regarding Ln(III) separation. The extraction kinetics was found to be fast as the extraction equilibrium is reached within 5-10 minutes (SI, Figure S24).

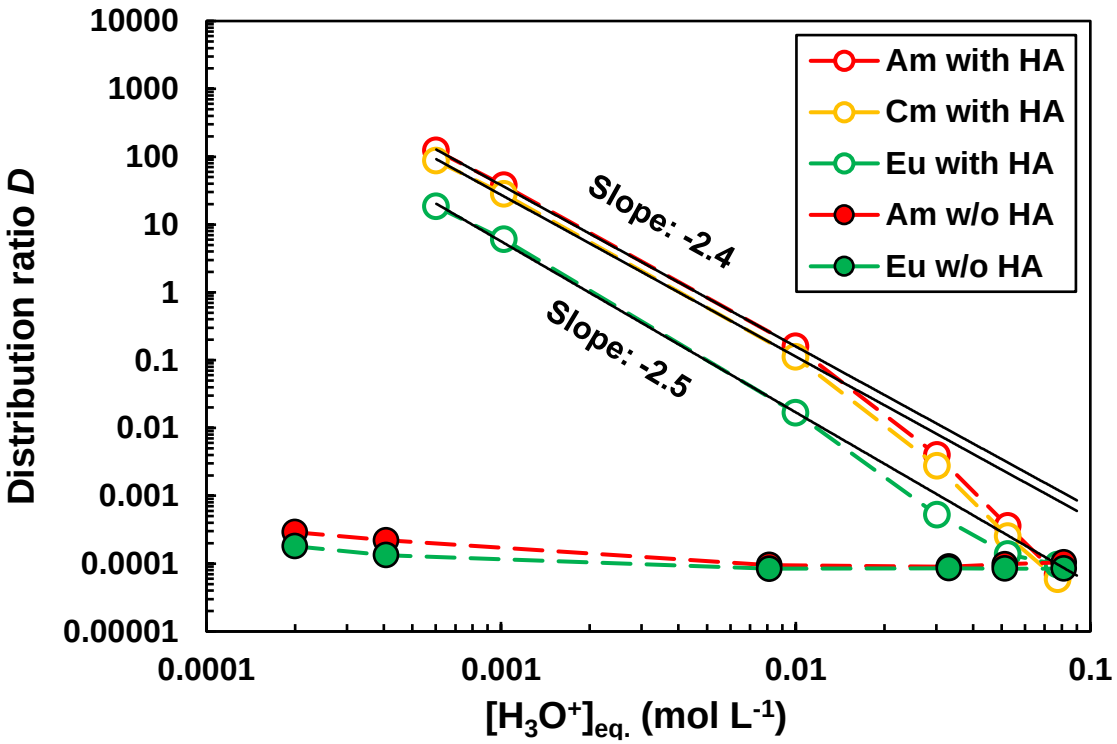

Figure 9: Distribution ratios of ^{152}Eu(III), ^{241}Am(III) and ^{244}Cm(III) as a function of the nitric acid concentration using 6.8 mmol L^{-1} MTB in tert-butylbenzene with (open symbols) or without (closed symbols) addition of 0.5 mol L^{-1} 2-bromodecanoic acid (HA).

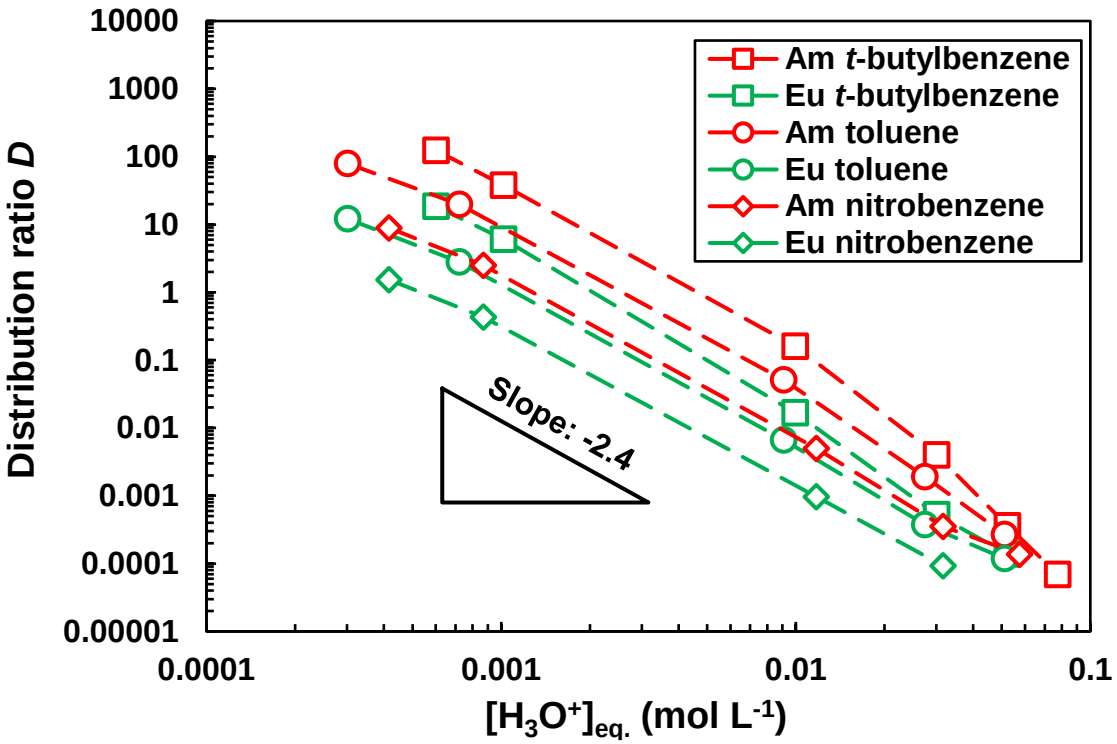

Figure 10: Distribution ratios of ^{152}Eu(III) and ^{241}Am(III) as a function of the HNO_3 concentration for extraction of 6.8 mmol L^{-1} MTB in tert-butylbenzene (□), 10 mmol L^{-1} MTB in toluene (○) and 10 mmol L^{-1} MTB in nitrobenzene (◊), each with addition of 0.5 mol L^{-1} 2-bromodecanoic acid.

The complex stoichiometry in the organic phase was studied using slope analysis of the metal distribution ratios as a function of the ligand concentration. Figure 11 shows the distribution ratios of La to Gd plus Y, Am, and Cm for MTB extraction in nitrobenzene (plus 0.5 mol L^{-1} HA) as a function of the MTB concentration at $pH_{eq.}$ = 3.1 ±0.1. Slopes of ca. 1.0 indicate the formation of a 1:1 (metal:ligand) complex. This is consistent with the crystal structures obtained for complexes **2-6**. In contrast, TRLFS studies in 2-propanol containing 50 vol.% H_2O, but without addition of a lipophilic anion source, show the formation of 1:1, 1:2 and 1:3 complexes with Cm. Deviations in the complex speciation for different solvents are likely.

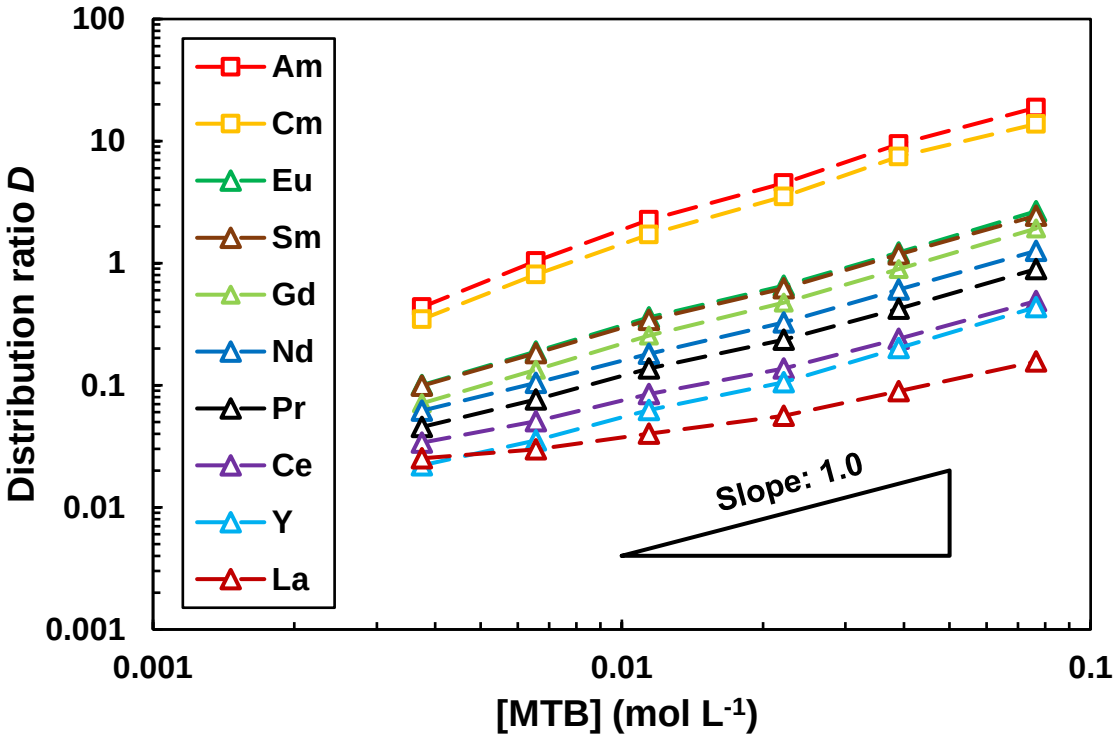

Figure 11: Distribution ratios of La(III) to Gd(III) (w/o Pm) plus Y(III), Am(III), and Cm(III) as a function of MTB concentration for extraction of MTB in nitrobenzene with addition of 0.5 mol L^{-1} 2-bromodecanoic acid at $pH_{eq.}$ 3.1 ±0.1.

Due to its solubility in nitric acid solutions, MTB was also considered as a hydrophilic complexing agent in combination with the well-established lipophilic An(III)/Ln(III) co-extracting agent *N,N,N',N'*-tetraoctyl diglycolamide (TODGA). Combining two ligands of different solubility and contrasting affinity is a common approach to enhance the overall selectivity.[45-48] The combination of TODGA in *n*-dodecane and MTB in nitric acid solution was tested. Due to the poor solubility of MTB in *n*-dodecane and its good solubility in nitric acid solutions (SI, Table S2), MTB remained in the aqueous phase indicated by the pink coloration (SI, Figure S25). However, at 4.1 mol L^{-1} HNO_3 the pink coloration vanished, probably caused by further protonation of MTB. Distribution ratios of Eu(III), Cm(III), and Am(III) for an extraction of TODGA in *n*-dodecane in combination with MTB in nitric acid solution were compared to data of TODGA extraction in the absence of MTB (SI, Figure S26). Distribution ratios were comparable for both extraction series, showing little effect regarding the addition

of MTB and no effect on the selectivity. It is assumed that at ≥ 0.1 mol L^{-1} HNO_3 protonated MTB is predominantly present, suppressing metal complexation with the free ligand, as already known from other hydrophilic N donor ligands.[49,50]

CONCLUSION

In this study, we presented a multi-method approach to investigate the complexation of 6-(6-methyl-1,2,4,5-tetrazine-3-yl)-2,2‘-bipyridine (MTB) with Ln(III) and An(III). As model complexes for the lanthanides, the six different complexes $[Ce(MTB)_2(NO_3)_3]$, $[Pr(MTB)(NO_3)_3H_2O]$, and $[Ln(MTB)(NO_3)_3MeCN]$ (Ln = Nd, Sm, Eu, Gd) with a ligand-to-metal ratio of 2:1 or 1:1 were synthesized. For the actinides, the complexation of Cm(III) with MTB was examined in solution using time-resolved laser fluorescence spectroscopy$[Cm(MTB)_{1\text{-}3}]^{3+}$ complexes with a ligand-to-metal ratio of 3:1, 2:1, and 1:1 were formed. Shifts of emission maxima of the different Cm(III) complex species were attributed to the existence of different configuration isomers of $[Cm(MTB)_n]^{3+}$ (n = 2-3) complexes, which was further investigated by quantum chemical calculations. Extraction studies showed that MTB separates An(III) from Ln(III) at low HNO_3 concentrations in presence of a lipophilic anion source. However, the determined separation factors are considerably smaller than in comparable N-donor systems. This might result from unfavorable complexation properties, as highlighted in an extensive spectroscopic study and by quantum chemical calculations of the complexation of MTB with trivalent metal ions. Nevertheless, the observed selectivity results from a stronger covalent contribution in the An-N interaction compared to the respective Ln-N interaction, as indicated by QTAIM analysis.

ASSOCIATED CONTENT

Supporting Information

The following files are available free of charge.

Synthesis and characterization, NMR and IR spectra, X-ray crystallography, and calculations (PDF)

AUTHOR INFORMATION

Corresponding Autor

Peter W. Roesky − Institut für Anorganische Chemie and Institute of Nanotechnology, Karlsruher Institut für Technologie, 76131 Karlsruhe, Germany; orcid.org/0000-0002-0915-3893;

Email: roesky@kit.edu

AUTHOR CONTRIBUTIONS

All authors have given approval to the final version of the manuscript. GG and TD synthesized and analyzed all compounds. PW conducted and interpreted the results of the TRLFS studies, RG the single crystal X-ray diffraction analysis, MP the computational results and FSS the solvent extraction studies. PWR originated the idea, supervised the work, and interpreted the results. All authors contributed to the preparation of the manuscript. All authors have given approval to the final version of the manuscript. ‡These authors contributed equally.

CONFLICTS OF INTEREST

There are no conflicts to declare.

ACKNOWLEDGMENT

Financial support for this research was provided by the German Federal Ministry of Education and Research through the *f*-Char project under grant numbers 02NUK059A, 02NUK059B, 02NUK059C, 02NUK059D and 02NUK059F.

References

(1) Matveev, P.; Mohapatra, P. K.; Kalmykov, S. N.; Petrov, V. Solvent extraction systems for mutual separation of Am (III) and Cm (III) from nitric acid solutions. A review of recent state-of-the-art. *Solvent Extr. Ion Exch.* **2021**, *39*, 679-713.

(2) Holdsworth, A. F.; Eccles, H.; Sharrad, C. A.; George, K. Spent Nuclear Fuel—Waste or Resource? The Potential of Strategic Materials Recovery during Recycle for Sustainability and Advanced Waste Management. *Waste* **2023**, *1*, 249-263.

(3) Lanham, W. B.; Runion, T. C., *Purex Process for Plutonium and Uranium Recovery*, Oak Ridge National Lab.(ORNL), Oak Ridge, TN (United States), 1949.

(4) Modolo, G.; Wilden, A.; Geist, A.; Magnusson, D.; Malmbeck, R. A review of the demonstration of innovative solvent extraction processes for the recovery of trivalent minor actinides from PUREX raffinate. *Radiochim. Acta* **2012**, *100*, 715-725.

(5) Geist, A.; Adnet, J.-M.; Bourg, S.; Ekberg, C.; Galán, H.; Guilbaud, P.; Miguirditchian, M.; Modolo, G.; Rhodes, C.; Taylor, R. An overview of solvent extraction processes developed in Europe for advanced nuclear fuel recycling, part 1-Heterogeneous recycling. *Sep. Sci. Technol.* **2021**, *56*, 1866-1881.

(6) Zsabka, P.; Wilden, A.; Van Hecke, K.; Modolo, G.; Verwerft, M.; Cardinaels, T. Beyond U/Pu separation: Separation of americium from the highly active PUREX raffinate. *J. Nucl. Mater.* **2023**, 154445.

(7) Taylor, R.; Mathers, G.; Banford, A. The development of future options for aqueous recycling of spent nuclear fuels. *Prog. Nucl. Energy* **2023**, *164*, 104837.

(8) Baron, P.; Cornet, S.; Collins, E.; DeAngelis, G.; Del Cul, G.; Fedorov, Y.; Glatz, J.; Ignatiev, V.; Inoue, T.; Khaperskaya, A. A review of separation processes proposed for advanced fuel cycles based on technology readiness level assessments. *Prog. Nucl. Energy* **2019**, *117*, 103091.

(9) Kolarik, Z. Complexation and separation of lanthanides(III) and actinides(III) by heterocyclic N-donors in solutions. *Chem. Rev.* **2008**, *108*, 4208-4252.

(10) Hudson, M. J.; Harwood, L. M.; Laventine, D. M.; Lewis, F. W. Use of soft heterocyclic N-donor ligands to separate actinides and lanthanides. *Inorg. Chem.* **2013**, *52*, 3414-3428.

(11) Panak, P. J.; Geist, A. Complexation and extraction of trivalent actinides and lanthanides by triazinylpyridine N-donor ligands. *Chem. Rev.* **2013**, *113*, 1199-1236.

(12) Wang, S.; Yang, X.; Liu, Y.; Xu, L.; Xu, C.; Xiao, C. Enhancing the Selectivity of Trivalent Actinide over Lanthanide Using Asymmetrical Phenanthroline Diamide Ligands. *Inorg. Chem.* **2024**, *63*, 3063-3074.

(13) Xu, L.; Yang, X.; Zhang, A.; Xu, C.; Xiao, C. Separation and complexation of f-block elements using hard-soft donors combined phenanthroline extractants. *Coord. Chem. Rev.* **2023**, *496*, 215404.

(14) Xiu, T.; Liu, L.; Liu, S.; Shehzad, H.; Liang, Y.; Zhang, M.; Ye, G.; Jiao, C.; Yuan, L.; Shi, W. Complexation and extraction of trivalent actinides over lanthanides using highly soluble phenanthroline diamide ligands with different side chains. *J. Hazard. Mater.* **2024**, *465*, 133508.

(15) Wu, Q.; Hao, H.; Liu, Y.; Sha, L.-T.; Wang, W.-J.; Shi, W.-q.; Wang, Z.; Yan, Z.-Y. Selective Separation of Americium (III), Curium (III), and Lanthanide (III) by Aqueous and Organic Competitive Extraction. *Inorg. Chem.* **2023**, *63*, 462-473.

(16) Ren, P.; Huang, P.-w.; Yang, X.-f.; Zou, Y.; Tao, W.-q.; Yang, S.-l.; Liu, Y.-h.; Wu, Q.-y.; Yuan, L.-y.; Chai, Z.-f. Hydrophilic sulfonated 2, 9-diamide-1, 10-phenanthroline endowed with a highly effective ligand for separation of americium (III) from europium (III): extraction, spectroscopy, and density functional theory calculations. *Inorg. Chem.* **2020**, *60*, 357-365.

(17) Wang, H.; Gao, P.; Cui, T.; Wang, D.; Liu, J.; He, H.; Chen, Z.; Jin, Q.; Guo, Z. New asymmetric tetradentate phenanthroline chelators with pyrazole and amide groups for complexation and solvent extraction of Ln (iii)/Am (iii). *Dalton Trans.* **2024**, *53*, 601-611.

(18) Kolarik, Z.; Müllich, U.; Gassner, F. Selective extraction of Am(III) over Eu(III) by 2,6-ditriazolyl- and 2,6-ditriazinylpyridines. *Solvent Extr. Ion Exch.* **1999**, *17*, 23-32.

(19) Trumm, S.; Geist, A.; Panak, P. J.; Fanghänel, T. An improved hydrolytically-stable Bis-Triazinyl-Pyridine (BTP) for selective actinide extraction. *Solvent Extr. Ion Exch.* **2011**, *29*, 213-229.

(20) Kolarik, Z.; Mullich, U.; Gassner, F. Extraction of Am (lll) and Eu (lll) nitrates by 2-6-di-(5, 6-dipropyl-1, 2, 4-triazin-3-yl) pyridines 1. *Solvent Extr. Ion Exch.* **1999**, *17*, 1155-1170.

(21) Drew, M. G. B.; Foreman, M. R. S. J.; Hill, C.; Hudson, M. J.; Madic, C. 6,6′-bis-(5,6-diethyl-[1,2,4]triazin-3-yl)-2,2′-bipyridyl the first example of a new class of quadridentate heterocyclic extraction reagents for the separation of americium(III) and europium(III). *Inorg. Chem. Commun.* **2005**, *8*, 239-241.

(22) Geist, A.; Hill, C.; Modolo, G.; Foreman, M. R. S. J.; Weigl, M.; Gompper, K.; Hudson, M. J.; Madic, C. 6,6′-Bis(5,5,8,8-tetramethyl-5,6,7,8-tetrahydro- benzo[1,2,4]triazin-3-yl) [2,2′]bipyridine, an effective extracting agent for the separation of americium(III) and curium(III) from the lanthanides. *Solvent Extr. Ion Exch.* **2006**, *24*, 463-483.

(23) Foreman, M. R. S. J.; Hudson, M. J.; Geist, A.; Madic, C.; Weigl, M. An investigation into the extraction of americium(III), lanthanides and D-block metals by 6,6′-bis-(5,6-dipentyl-[1,2,4]triazin-3-yl)- [2,2′]bipyridinyl (C5-BTBP). *Solvent Extr. Ion Exch.* **2005**, *23*, 645-662.

(24) Lewis, F. W.; Harwood, L. M.; Hudson, M. J.; Drew, M. G. B.; Desreux, J. F.; Vidick, G.; Bouslimani, N.; Modolo, G.; Wilden, A.; Sypula, M.; Vu, T. H.; Simonin, J. P. Highly efficient separation of actinides from lanthanides by a phenanthroline-derived bis-triazine ligand. *J. Am. Chem. Soc.* **2011**, *133*, 13093-13102.

(25) Lewis, F. W.; Harwood, L. M.; Hudson, M. J.; Drew, M. G.; Wilden, A.; Sypula, M.; Modolo, G.; Vu, T.-H.; Simonin, J.-P.; Vidick, G. From BTBPs to BTPhens: the effect of ligand pre-organization on the extraction properties of quadridentate bis-triazine ligands. *Procedia Chem.* **2012**, *7*, 231-238.

(26) Deblonde, G. J.-P.; Chagnes, A.; Cote, G. Recent advances in the chemistry of hydrometallurgical methods. *Separation & Purification Reviews* **2023**, *52*, 221-241.

(27) Ermolaev, S. V.; Vasiliev, A. N.; Lapshina, E. V.; Kobtsev, A. A.; Zhuikov, B. L. Production of 225 Ac for medical application from 232 Th-metallic targets in Nb-shells irradiated with middle-energy protons. *New J. Chem.* **2024**, *48*, 8222-8232.

(28) Kratsch, J.; Beele, B. B.; Koke, C.; Denecke, M. A.; Geist, A.; Panak, P. J.; Roesky, P. W. 6-(Tetrazol-5-yl)-2,2′-bipyridine: A highly selective ligand for the separation of lanthanides(III) and actinides(III). *Inorg. Chem.* **2014**, *53*, 8949-8958.

(29) Zhu, Z. H.; Li, Y.; Wang, Y. B.; Lan, Z. G.; Zhu, X.; Hao, X. Q.; Song, M. P. α-Alkylation of Nitriles with Alcohols Catalyzed by NNN′ Pincer Ru(II) Complexes Bearing Bipyridyl Imidazoline Ligands. *Organometallics* **2019**, *38*, 2156-2166.

(30) Fife, W. K. Regioselective Cyanation of Pyridine 1-Oxides with Trimethylsilanecarbonitrile: A Modified Reissert-Henze Reaction. *J. Org. Chem.* **1983**, *48*, 1375-1377.

(31) Maiwald, M. M.; Wagner, A. T.; Kratsch, J.; Skerencak-Frech, A.; Trumm, M.; Geist, A.; Roesky, P. W.; Panak, P. J. 4,4′-Di-tert -butyl-6-(1 H -tetrazol-5-yl)-2,2′-bipyridine: Modification of a highly selective N-donor ligand for the separation of trivalent actinides from lanthanides. *Dalton Trans.* **2017**, *46*.

(32) Polezhaev, A. V.; Maciulis, N. A.; Chen, C. H.; Pink, M.; Lord, R. L.; Caulton, K. G. Tetrazine Assists Reduction of Water by Phosphines: Application in the Mitsunobu Reaction. *Chem. Eur. J.* **2016**, *22*, 13985-13998.

(33) Shannon, R. D. Revised effective ionic radii and systematic studies of interatomic distances in halides and chalcogenides. *Acta Crystallogr. Sect. A: Found. Crystallogr.* **1976**, *32*, 751-767.

(34) Bremer, A.; Müllich, U.; Geist, A.; Panak, P. J. Influence of the solvent on the complexation of Cm(III) and Eu(III) with nPr-BTP studied by time-resolved laser fluorescence spectroscopy. *New J. Chem.* **2015**, *39*, 1330-1338.

(35) Bremer, A.; Geist, A.; Panak, P. J. Complexation of Cm(iii) with 6-(5,6-dipentyl-1,2,4-triazin-3-yl)-2, 2′-bipyridine studied by time resolved laser fluorescence spectroscopy. *Dalton Trans.* **2012**, *41*, 7582-7589.

(36) Beele, B. B.; Rüdiger, E.; Schwörer, F.; Müllich, U.; Geist, A.; Panak, P. J. A TRLFS study on the complexation of novel BTP type ligands with Cm(iii). *Dalton Trans.* **2013**, *42*, 12139-12147.

(37) Weßling, P.; Trumm, M.; Sittel, T.; Geist, A.; Panak, P. J. Spectroscopic investigation of the different complexation and extraction properties of diastereomeric diglycolamide ligands. *Radiochim. Acta* **2022**, *110*, 291-300.

(38) Preston, J. S. Solvent extraction of the trivalent lanthanides and yttrium by some 2-bromoalkanoic acids. *Solvent Extr. Ion Exch.* **1994**, *12*, 29-54.

(39) Hagström, I.; Spjuth, L.; Enarsson, A.; Liljenzin, J. O.; Skalberg, M.; Hudson, M.; Iveson, P., B.; Madic, C.; Cardiel, P. Y.; Hill, C.; Francois, N. Synergistic solvent extraction of trivalent americium and europium by 2-bromodecanoic acid and neutral nitrogen-containing reagents. *Solvent Extr. Ion Exch.* **1999**, *17*, 221-242.

(40) Hudson, M.; Liljenzin, J. O.; Nilsson, M.; Skarnemark, G.; Spahiu, K.; Andersson, S.; Ekberg, C.; Foreman, M. Extraction Behavior of the Synergistic System 2,6-bis-(Benzoxazolyl)-4- Dodecyloxylpyridine and 2-Bromodecanoic Acid Using Am and Eu as Radioactive Tracers. *Solvent Extr. Ion Exch.* **2003**, *21*, 621-636.

(41) Bremer, A.; Ruff, C. M.; Girnt, D.; Müllich, U.; Rothe, J.; Roesky, P. W.; Panak, P. J.; Karpov, A.; Müller, T. J. J.; Denecke, M. A.; Geist, A. 2, 6-Bis (5-(2, 2-dimethylpropyl)-1 H-pyrazol-3-yl) pyridine as a ligand for efficient actinide (III)/lanthanide (III) separation. *Inorg. Chem.* **2012**, *51*, 5199-5207.

(42) Wilden, A.; Modolo, G.; Kaufholz, P.; Sadowski, F.; Lange, S.; Munzel, D.; Geist, A. Process Development and Laboratory-scale Demonstration of a regular-SANEX Process Using C5-BPP (2,6-Bis(5-(2,2-dimethylpropyl)-1H-pyrazol-3-yl)pyridine). *Sep. Sci. Technol.* **2015**, *50*, 2467-2475.

(43) Nilsson, M.; Andersson, S.; Ekberg, C.; Liljenzin, J. O.; Skarnemark, G. Chemical Properties of 2-Bromodecanic Acid. *Solvent Extr. Ion Exch.* **2006**, *24*, 407 -418.

(44) Beele, B. B.; Müllich, U.; Schwörer, F.; Geist, A.; Panak, P. J. Systematic Modifications of BTP-type Ligands and Effects on the Separation of Trivalent Lanthanides and Actinides. *Procedia Chem.* **2012**, *7*, 146-151.

(45) Geist, A.; Müllich, U.; Magnusson, D.; Kaden, P.; Modolo, G.; Wilden, A.; Zevaco, T. Actinide(III)/Lanthanide(III) Separation Via Selective Aqueous Complexation of Actinides(III) using a Hydrophilic 2,6-Bis(1,2,4-Triazin-3-Yl)-Pyridine in Nitric Acid. *Solvent Extr. Ion Exch.* **2012**, *30*, 433-444.

(46) Wagner, C.; Müllich, U.; Geist, A.; Panak, P. J. Selective Extraction of Am(III) from PUREX Raffinate: The AmSel System. *Solvent Extr. Ion Exch.* **2016**, *34*, 103-113.

(47) Macerata, E.; Mossini, E.; Scaravaggi, S.; Mariani, M.; Mele, A.; Panzeri, W.; Boubals, N.; Berthon, L.; Charbonnel, M.-C.; Sansone, F.; Arduini, A.; Casnati, A. Hydrophilic Clicked 2,6-Bis-triazolyl-pyridines Endowed with High Actinide Selectivity and Radiochemical Stability: Toward a Closed Nuclear Fuel Cycle. *J. Am. Chem. Soc.* **2016**, *138*, 7232-7235.

(48) Weßling, P.; Maag, M.; Baruth, G.; Sittel, T.; Sauerwein, F. S.; Wilden, A.; Modolo, G.; Geist, A.; Panak, P. J. Complexation and Extraction Studies of Trivalent Actinides and Lanthanides with Water-Soluble and CHON-Compatible Ligands for the Selective Extraction of Americium. *Inorg. Chem.* **2022**, *61*, 17719-17729.

(49) Weßling, P.; Trumm, M.; Macerata, E.; Ossola, A.; Mossini, E.; Gullo, M. C.; Arduini, A.; Casnati, A.; Mariani, M.; Adam, C.; Geist, A.; Panak, P. J. Activation of the Aromatic Core of 3, 3′-(Pyridine-2, 6-diylbis (1 H-1, 2, 3-triazole-4, 1-diyl)) bis (propan-1-ol)—Effects on Extraction Performance, Stability Constants, and Basicity. *Inorg. Chem.* **2019**, *58*, 14642-14651.

(50) Edwards, A. C.; Mocilac, P.; Geist, A.; Harwood, L. M.; Sharrad, C. A.; Burton, N. A.; Whitehead, R. C.; Denecke, M. A. Hydrophilic 2,9-bis-triazolyl-1,10-phenanthroline ligands

enable selective Am(III) separation: a step further towards sustainable nuclear energy. *Chem. Commun.* **2017**, *53*, 5001-5004.

TOC

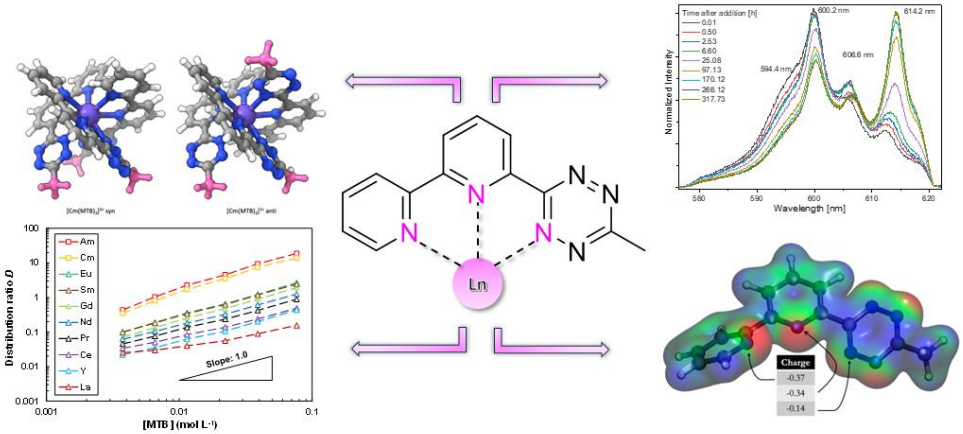

The N-donor ligand 6-(6-methyl-1,2,4,5-tetrazin-3-yl)-2,2'-bipyridine (MTB), developed for the separation of trivalent actinides (An) from lanthanides (Ln), was synthesized and studied with trivalent lanthanides and actinides. Six lanthanide complexes were obtained. Solvent extraction studies show a slight selectivity for Am and Cm over Ln and indicate 1:1 complex formation. Studies with Cm by time-resolved laser fluorescence spectroscopy show three different complex types and two isomers in solution, which is confirmed by quantum chemical calculations.